RESEARCH ARTICLE | AUGUST 01 1988

Self-focusing and ion wave generation in laser-produced plasmas

R. Rankin; R. Marchand; C. E. Capjack

Phys. Fluids 31, 2327–2334 (1988)
https://doi.org/10.1063/1.866633

Self-focusing and ion wave generation in laser-produced plasmas

R. Rankin, R. Marchand, and C. E. Capjack
Department of Electrical Engineering, University of Alberta, Edmonton, Alberta T6G 2G7, Canada

(Received 4 December 1987; accepted 7 April 1988)

Two-dimensional hydrodynamic simulations of laser light self-focusing in a hydrogen plasma are presented. The simulation code includes a model for laser beam propagation which accounts for inverse bremsstrahlung absorption, refraction, diffraction, and ponderomotive forces. A Gaussian hot spot, superimposed upon a collimated, spatially uniform laser beam, is used to initiate self-focusing. Intense filaments provide a driving source for ion waves near the axis of the laser beam. The radially propagating ion waves cause spatiotemporal modulations of the flux where it is initially uniform, as well as the more usual focusing that occurs along the axis. Some of the factors affecting the generation of the ion waves are considered. In particular, the effect of changing the amplitude and width of the imposed nonuniformity is investigated. The intensity thresholds for thermal and ponderomotively driven self-focusing have also been determined by artificially turning the ponderomotive force on and off.

I. INTRODUCTION

Self-focusing of high intensity laser light poses a serious threat to the feasibility of directly driven compressions required for inertial confinement fusion. This is particularly true for the long scale length (millimeter length) plasmas envisaged for reactor conditions. The recent interest in short wavelength lasers ($\lambda \sim 0.25\ \mu$m) is motivated by the expectation that anomalous scattering and absorption processes will be less important as mechanisms for degrading the laser–plasma coupling efficiency. If filamentation of the incident laser light occurs, however, these processes may reappear. In particular, the high intensity of the filamented light can exceed threshold conditions for parametric instabilities and may be a source of suprathermal electrons.[1–14] The filamented light can also break up the implosion uniformity of the target plasma, resulting in a reduction in compression. In this context, it is vital to consider the physical processes that influence self-focusing of the incident light wave.

In the past several years, there have been a number of studies of filamentation in laser-produced plasmas, both from an analytical point of view,[15–19] and by using numerical simulation codes.[20–25] In this paper, a two-dimensional Eulerian hydrodynamic simulation code is used to investigate self-focusing. As well as solving the plasma fluid equations, the code includes a calculation of laser beam propagation and energy deposition. This is accomplished by solving the laser light paraxial wave equation numerically. The advantage of this approach is that diffraction and ponderomotive force terms can be accounted for. As a result of their complexity, these effects are normally neglected in ray-tracing calculations, although they can affect self-focusing of the laser beam appreciably. In particular, diffraction and ponderomotive forces become important when the laser beam is tightly focused or modulated, or when large field gradients develop. Ray tracing has intrinsic advantages for describing hydrodynamic implosion calculations, but filamentation in subcritical density plasmas is more accurately described by the paraxial wave approach.

In the work reported here, we have assessed the relative importance of thermal versus ponderomotive self-focusing in a hydrogen plasma. Rather than study whole-beam self-focusing, we have chosen to study the focusing that results from the superposition of a Gaussian hot spot with a plane uniform laser beam of constant intensity. This is considered to be a more realistic initial condition for self-focusing than would be a whole-beam Gaussian intensity distribution.

The simulation code has been used to investigate thermal (TH) and ponderomotive force (PF) self-focusing at plasma densities varying from $0.1n_c$ to $0.3n_c$ [n_c (m^{-3}) $= 1.1\times 10^{27}\lambda_L^{-2}$ (μm) is the critical density for the incident light wave], and at temperatures ranging from 1 keV to 5 keV. Threshold intensities for self-focusing have been determined as a function of the radius of the Gaussian hot spot. Results are presented with the PF included, and with it artificially turned off. This enables TH and PF self-focusing to be distinguished. Small-scale self-focusing is also investigated. Recently, we reported evidence of small-scale filamentary structures in simulations involving hydrogen plasmas.[26] Typically, the simulations showed ion waves moving radially away from the laser beam axis, where the imposed nonuniform energy deposition occurs. These ion waves cause refraction of incoming light waves, and result in the initially spatially uniform portion of the beam becoming nonuniform. These nonuniformities will eventually be impressed on the ablation front, thus degrading compression and causing mixing of the target fuel elements. In a recent analysis of the problem, Coggeshall *et al.*[27] also reported ion-wave fluctuations and small-scale focusing. They have referred to the small-scale focusing as "flickering." In their analysis, the beam is modeled with the equations of geometrical optics, and the effects of diffraction, divergence of the plasma flow, and the ponderomotive force are assumed to be negligible. These effects are included in the present study.

The paper is divided into the following sections. A brief description of the physical model assumed in the simulations is given in Sec. II. In Sec. III, intensity threshold dependences of TH and PF self-focusing are presented, and in Sec. IV small-scale self-focusing is described. Section V contains a summary of the results together with concluding remarks.

 0031-9171/88/082327-08$01.90

II. PHYSICAL MODEL

A two-dimensional cylindrically symmetric Eulerian plasma simulation code is used to investigate laser light self-focusing. The methodology used in the development of this code is described elsewhere,[28] therefore only a brief description of the physical processes modeled is given here. The code is comprised of (i) a laser beam propagation module, (ii) an electron–ion temperature diffusion and equilibration package, (iii) a module that solves the plasma fluid equations, and (iv) a model equation of state.

The laser routine accounts for absorption, refraction, diffraction, and ponderomotive forces.[29] Given the electron density n_e and temperature T_e over the simulation mesh, the paraxial wave equation is solved by approximating the radial flux with cubic splines, and by using conservative spatial differencing in the axial (z) direction. The laser energy deposited in each fluid cell acts as a source term in the electron temperature equation. The electron–ion temperature diffusion and equilibration equations are then solved simultaneously using the incomplete Cholesky conjugate gradient method described by Kershaw.[30] A simultaneous solution is necessary in order to prevent a numerical instability caused by the exchange term in these equations.[28] The ponderomotive and $p\Delta V$ work terms are used as source terms in the plasma fluid equations, which are solved numerically using the flux-corrected transport algorithm of Boris.[31] This method of solution ensures that steep density gradients can be accurately described. The temperature range investigated permits the use of a perfect gas equation of state model.

Since the laser routine forms an important part of the present calculation, it is more fully discussed here. Specifically, the solution of the paraxial wave equation

$$\frac{\partial \mathbf{F}}{\partial z} = \frac{i}{2k}\left[\frac{1}{r}\frac{\partial}{\partial r}\left(r\frac{\partial \mathbf{F}}{\partial r}\right) - q^2(r,z)\mathbf{F}(r,z)\right] \tag{1}$$

is required. It is assumed that the laser beam is cylindrically symmetric, and Eq. (1) is in terms of the cylindrical coordinates r and z. The electric field $\mathbf{E}(r,z)$ is related to the complex flux amplitude $\mathbf{F}(r,z)$ by

$$\mathbf{E}(r) = \left(\frac{8\pi}{c^2 k(z)}\right)^{1/2}\mathbf{F}(r,z)\exp i\int_0^z k(z')dz' . \tag{2}$$

The quantity $q^2(r,z)$ is defined by the expression

$$q^2(r,z) = (1/c^2)\{[\omega_p^2(r,z) - \omega_p^2(0,z)] - i\omega_p^2(r,z)\nu_c(r,z)/\omega\} . \tag{3}$$

The first term on the right-hand side of Eq. (1) describes diffraction of the beam whereas the first term in the equation for $q^2(r,z)$ describes refraction and the second term accounts for inverse bremsstrahlung absorption. Equation (1) is solved numerically by approximating the r dependence of the flux with cubic splines, as described by Fleck.[32] The z derivative is approximated by a conservative finite difference scheme, and is such that the flux on the boundary at $z = 0$ determines the flux at all subsequent z positions in the plasma. Mathematically, the incident laser intensity on the boundary (at $z = 0$) is described by $I(r,z=0) = I_0(1 + \epsilon e^{-r^2/\sigma^2})$, with $I_0 = 10^{15}$ Wcm^{-2}, and σ and ϵ as variable parameters.

III. INTENSITY THRESHOLD CALCULATIONS

In the following examples, we describe the results of a number of simulations of laser beam filamentation in a low density hydrogen plasma. Our aim is to assess the relative importance of TH versus PF self-focusing in the outer corona of a plasma which has been irradiated by laser light with a wavelength of 0.25 μm. We have considered self-focusing taking place within a prescribed parameter range, namely, at densities between $0.1n_c$ and $0.3n_c$, and at temperatures ranging from 1 keV to 5 keV. The plasma is initially spatially uniform and the background intensity is always chosen to be 10^{15} Wcm^{-2}. Self-focusing is investigated by varying the amplitude (ϵ) and radius (σ) of the Gaussian hot spot, and by artificially turning the ponderomotive force on or off. By changing the plasma density and temperature, it is possible to examine regimes in which ponderomotive or thermal self-focusing dominates.

In Figs. 1–7, we consider threshold intensities that cause the incident laser beam to self-focus within the volume of plasma simulated. For each set of parameters used, the length of plasma is adjusted to ensure that the intensity is attenuated by at least a factor of 100. Since the time scale for self-focusing depends upon the chosen plasma parameters and on the incident laser intensity, we have restricted our calculations to focusing taking place within a fixed time interval. This is sufficient to enable comparisons to be made of the relative strength of thermal versus ponderomotive self-focusing. Specifically, we have chosen a time frame of 1.5 nsec in which to look for self-focusing. This is considered to be realistic when compared to the time scale for hydrodynamic motion. In the figures, the shaded areas define boundaries that indicate the parameter range where self-focusing first takes place. The finite width of this region is affected by the fact that a finite number of computer runs have been used to determine values of ϵ that will cause the beam to self-focus. To be specific, in Fig. 1 the lower marker symbols show, for a given spot size, the largest value of ϵ that failed to produce self-focusing. The upper marker symbols show the intensity fractions that cause the beam to self-focus to greater than four times its initial intensity.

Figure 1 shows results for a plasma with a density of $0.1n_c$ and temperatures $T_e = T_i = 5$ keV. The ponderomotive force is artificially set to zero for the examples presented. Figure 1 shows the Gaussian intensity (expressed as a fraction of the uniform background intensity) necessary to drive self-focusing. The results were obtained from simulations using initial beam radii of 50 μm, 100 μm, and 150 μm. It can be seen that larger spot sizes self-focus at lower intensities. This occurs because heat diffusion becomes important when the radius of the hot spot is reduced. Clearly, at 5 keV, it is difficult for filaments to form when the hot spot has a radius less than 100 μm. For the 100 μm and 150 μm radius hot spots, filaments form when ϵ is between 15 and 20, whereas at 50 μm filaments form with an ϵ of 40. These results indicate that at 5 keV thermal self-focusing is relatively weak.

The effect of reducing the plasma temperature to 2.5 keV is shown in Fig. 2. In this case, the threshold intensities are approximately 20 times lower than those required at 5 keV. For the 100 μm and 150 μm spot sizes, the thresholds

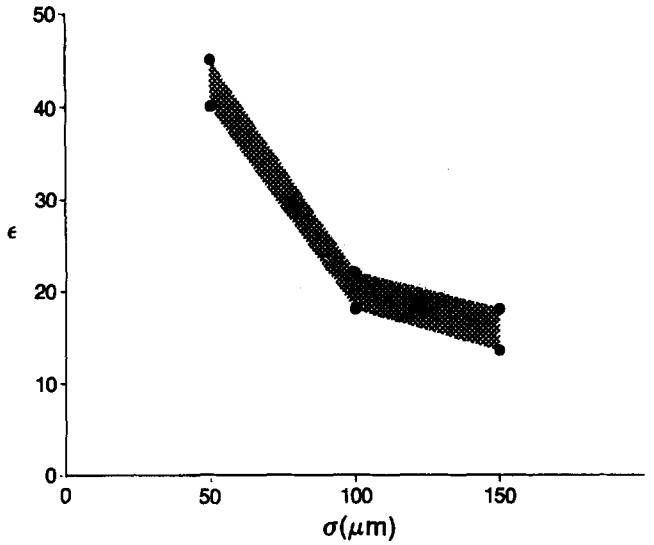

FIG. 1. The intensity of the hot spot (expressed as a fraction of the uniform background intensity of 10^{15} Wcm^{-2}) required for self-focusing to occur. Here, $n_e/n_c = 0.1$, $T_e = T_i = 5$ keV, PF turned off.

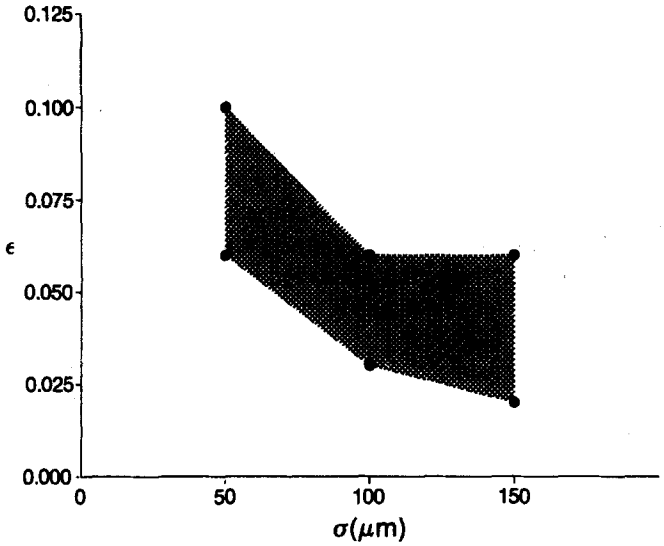

FIG. 3. Same as in Fig. 1 except that $T_e = T_i = 1$ keV, PF turned off.

are approximately equal. The 150 μm spot size starts to focus at the lowest intensity, but an ϵ of unity gives approximately the same intensity multiplication for both spot sizes. Diffusion still remains important for the 50 μm spot size at this temperature and density, as the threshold curve clearly demonstrates.

In Fig. 3, the temperature has been reduced further to 1 keV. This temperature would be more typical of the values attained in present day experiments with 0.25 μm wavelength laser light. The same overall behavior occurring in Figs. 1 and 2 is evident here. Now, however, only a very modest ($< 10\%$) intensity modulation is required to induce self-focusing. The intensity thresholds are approximately 20 times lower than those shown in Fig. 2. It is interesting to note that at this temperature and density, self-focusing is relatively insensitive to the magnitude of ϵ once the threshold intensity is exceeded. For example, it is necessary to double the value of ϵ at which focusing first occurs, to increase the focused intensity significantly. This is in contrast to the results at higher temperature, where a small change in ϵ increased the focused intensity significantly. Figures 1–3 indicate a strong dependence of thermal self-focusing on the initial plasma temperature. The threshold intensity increases by approximately three orders of magnitude as the temperature is changed from 1 keV to 5 keV. As expected, when T_e is reduced diffusion becomes important at smaller values of σ. This is illustrated by the steady decrease in the slope of the threshold curves, between $\sigma = 50$ μm and $\sigma = 100$ μm, as T_e is changed from 5 keV (Fig. 1) to 1 keV (Fig. 3). This behavior is summarized in Fig. 4, where ϵ for the three σ values is plotted as a function of T_e.

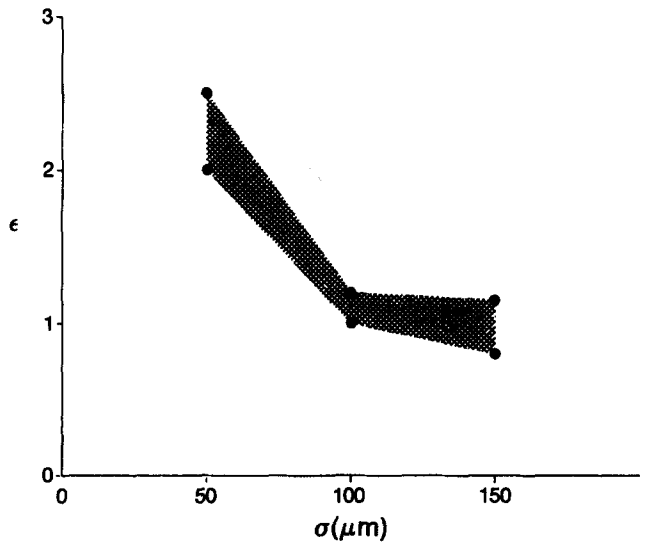

FIG. 2. Same as in Fig. 1 except that $T_e = T_i = 2.5$ keV, PF turned off.

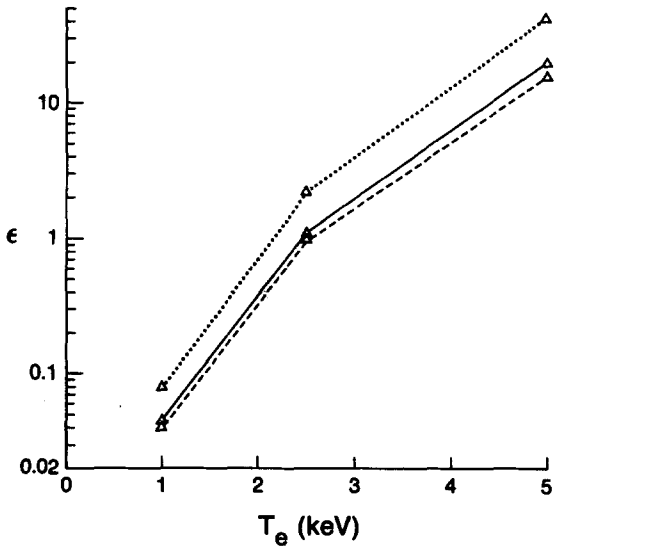

FIG. 4. The intensity of the hot spot (expressed as a fraction of the uniform background intensity of 10^{15} Wcm^{-2}) as a function of T_e, for (a) $\sigma = 50$ μm dotted line, (b) $\sigma = 100$ μm solid line, (c) $\sigma = 150$ μm dashed line.

It is of interest to examine the threshold dependence of self-focusing when the ponderomotive force is included in the calculation. The results shown in Fig. 5 use the same parameters as Fig. 1, i.e., $T_e = 5$ keV, and $n_e = 0.1 n_c$. Note that, in contrast to Fig. 1, the intensity threshold increases with the spot size. This is because the ponderomotive force is smaller when the spot size is increased, with the result that smaller amplitude density channels form. The refraction of laser light into these channels is reduced, and a higher intensity is needed for self-focusing to occur within the prescribed 1.5 nsec time frame.

A comparison of Fig. 1 with Fig. 5 makes it clear that self-focusing is driven by the PF for the initial density and temperature described above. When σ is 100 μm, for example, the ratio of TH to PF threshold intensities is 1:200, whereas at 50 μm this figure is increased to 1:5000. Figures 1–3 show that thermal self-focusing becomes increasingly more important when the initial plasma temperature is small. For example, Fig. 3 (TH self-focusing only) and Fig. 5 (PF self-focusing) show that TH self-focusing, at $T_e = 1$ keV, $n_e = 0.1 n_c$, and $\sigma > 50$ μm, is comparable to PF self-focusing at $T_e = 5$ keV. This is not the case at smaller values of σ, and we conclude that hot spots with $\sigma \leq 50$ μm, will self-focus in the outer corona (where $n_e \leq 0.1 n_c$) caused primarily by the ponderomotive force.

From a physical point of view, thermal self-focusing is expected to become important (relative to ponderomotive self-focusing) at higher densities, since temperature diffusion out of the heated region is reduced, and absorption of laser energy is greater. The case shown in Fig. 6 is for $T_e = T_i = 1$ keV, and $n_e = 0.3 n_c$. The density is three times larger than the value previously used. The first point to notice is that the threshold intensity slope does not jump between $\sigma = 50$ μm and $\sigma = 100$ μm, as it did at the lower density used. At higher density, energy diffusion becomes less important for the spot sizes used. Diffusion would be expected to become more important at smaller values of σ, i.e., $\sigma < 50$ μm, but we have not pursued this point further.

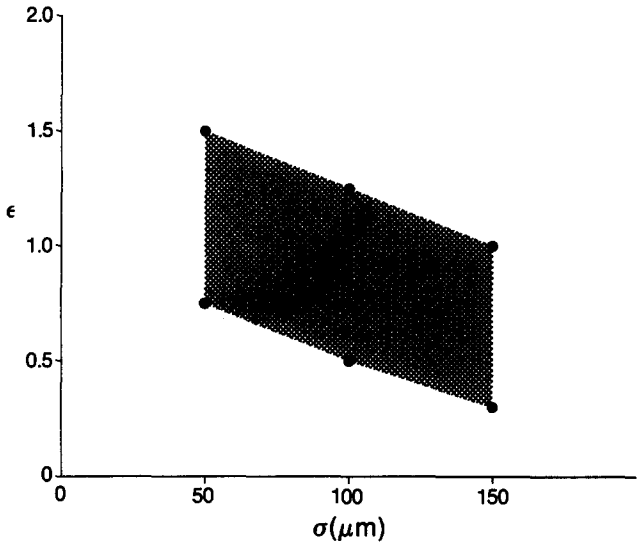

FIG. 6. Same as in Fig. 1 except that $n_e/n_c = 0.3$, $T_e = T_i = 1$ keV, PF turned off.

The second point to notice is that the intensity thresholds are higher than the corresponding values on Fig. 3. This contradicts our earlier statement about thermal self-focusing being more important at higher density. However, the laser light is being strongly attenuated as it propagates through the plasma, so that although the focusing may be stronger, it requires a higher initial intensity to enable the beam to have a finite value at the focus.

In Fig. 7, we examine the effect of the ponderomotive force at the higher density of $0.3 n_c$. The results will be compared to the lower density results ($0.1 n_c$) shown in Fig. 5, since in both cases a 5 keV initial plasma temperature is assumed. In Fig. 5, the PF was shown to be the dominant driving term for self-focusing. This is also the case when the density is $0.3 n_c$. However, the threshold intensities are higher than those required at $0.1 n_c$. On comparing both sets of

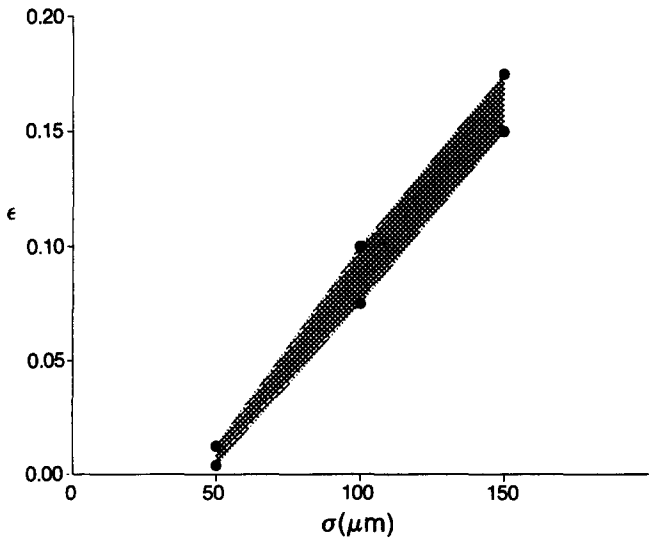

FIG. 5. Same as in Fig. 1 except that $T_e = T_i = 5$ keV, PF turned on.

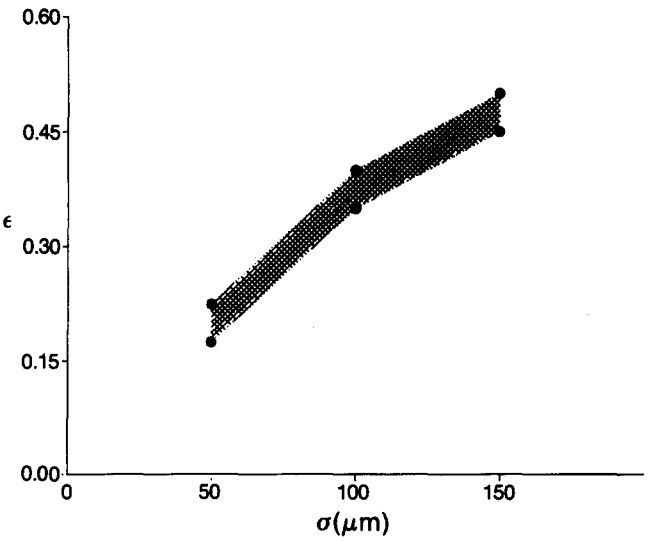

FIG. 7. Same as in Fig. 1 except that $n_e/n_c = 0.3$, $T_e = T_i = 5$ keV, PF turned on.

results, it can be seen that the intensity thresholds for the three values of σ used must be multiplied (approximately) by 2.9 for $\sigma = 150\,\mu$m, by 4.3 for $\sigma = 100\,\mu$m, and by 24.2 for $\sigma = 50\,\mu$m. The threshold intensity for self-focusing is higher at $0.3n_c$ because of increased laser beam attenuation caused by inverse bremsstrahlung absorption. The significant increase in the threshold intensity at $\sigma = 50\,\mu$m (when the density is raised) indicates that small radius hot spots are more effective at driving filamentation in low density plasmas.

IV. SMALL-SCALE SELF-FOCUSING

In this section, the effect of small-scale ion wave fluctuations on laser beam filamentation is examined. The first simulation considered is one in which the laser beam is propagated through a plasma that has an initial temperature of 5 keV. A Gaussian beam with an amplitude equivalent to 50% of the uniform intensity background (i.e., $\epsilon = 0.5$), and a σ of 100 μm, is assumed. Plots of the laser flux after four time intervals are shown in Fig. 8. In the figure, the beam enters the plasma at $z = 0$ and propagates in the direction of increasing z. Because of the cylindrical coordinate system, the figures are symmetric about the z axis. Note that inverse bremsstrahlung absorption serves to attenuate the laser flux as the beam propagates in the direction of increasing z. Figure 8(a) shows the onset of self-focusing. Note that the beam is beginning to break up into a number of filaments, although the predominant focusing occurs close to $r = 0$.

In Fig. 8(b), the beam focuses strongly inside the Gaussian spot. As well as on-axis focusing, the flux is modulated off-axis. This is particularly evident in Figs. 8(c) and 8(d). On comparing these figures, it can be seen that the off-axis disturbances are moving outwards away from the z axis. This is caused by ion wave generation within the nonuniform part of the incident beam. By examining a time sequence of the data used to obtain the figures shown, we have determined that these structures are moving at approximately the sound speed. The perturbations in the flux are caused by refraction of laser light in the propagating ion density depressions. These density depressions serve to magnify the laser flux in the direction of the laser beam. However, the ion waves are transient relative to the time scale for self-focusing: the transit time of a sound wave across the 1 mm radius plasma is approximately 1.5 nsec whereas in this particular simulation the time scale for self-focusing is approximately 0.5 nsec. The ion waves can therefore move a significant distance radially on the time scale for self-focusing, so that a large off-axis flux amplification does not occur.

An inspection of Figs. 1 and 5 shows that the ponderomotive force is responsible for the focusing occurring in Fig. 8. For example, when $\sigma = 100\,\mu$m, and $T_e = 5$ keV, an ϵ of

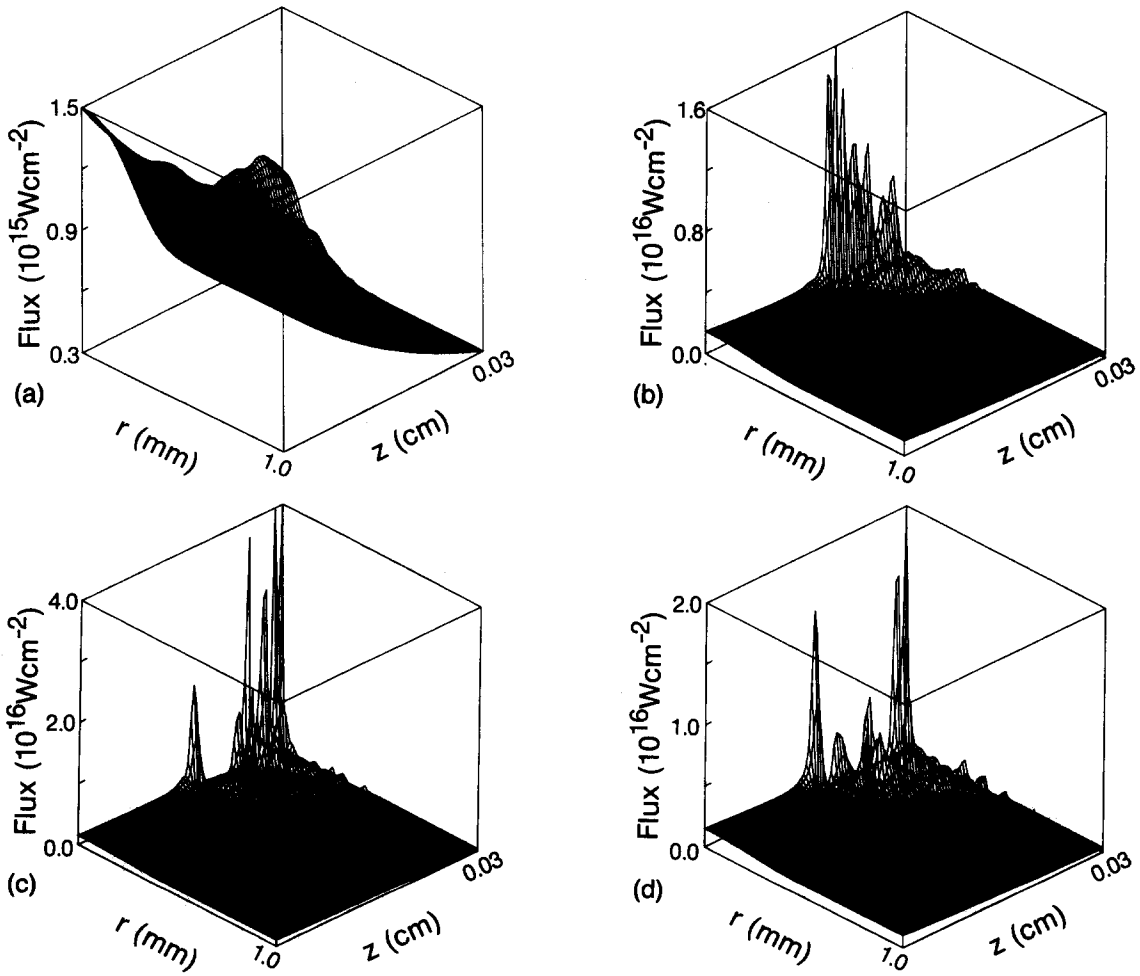

FIG. 8. Flux versus r and z for a Gaussian wave superimposed upon uniform plane laser light. Parameters used are (i) uniform intensity of 10^{15} Wcm^{-2}, (ii) $T_e = T_i = 5$ keV, (iii) $n_e/n_c = 0.1$, (iv) $\sigma = 100\,\mu$m, (v) $\epsilon = 0.5$. The flux is shown at (a) $t = 0.581$ nsec, (b) $t = 0.745$ nsec, (c) $t = 0.988$ nsec, (d) $t = 1.07$ nsec.

20 is required for thermal self-focusing to occur. For the same parameters, ponderomotive self-focusing first takes place when $\epsilon = 0.1$. Therefore, in Fig. 8 the initial intensity exceeds the PF intensity threshold by a factor of 5. More generally, at $T_e = 5$ keV, filamentation is driven by the ponderomotive force for all of the spot sizes considered.

We have also investigated the effect of changing the amplitude and width of the Gaussian beam. The main effect of increasing the amplitude is that it decreases the time scale for on-axis self-focusing to occur. Provided the incident intensity is large enough for self-focusing to take place, we still observe intensity modulations off-axis. For example, a 10% nonuniformity in the incident flux still results in off-axis intensity variations similar to those of Fig. 8. No significant differences are observed for the three spot sizes used. The amplitude of the Gaussian at which self-focusing first occurs increases with the spot size, but again, provided the intensity is above threshold, the PF can focus the beam down to a very narrow waist. The simulations indicate that this causes ion waves to be generated.

In the examples discussed above, it was shown that the PF was the driving source for self-focusing and ion wave generation. It is now of interest to consider some of the features that characterize thermal self-focusing. This can be accomplished by artificially turning off the ponderomotive force in the simulations, or, more realistically, by investigating a parameter range in which thermal self-focusing is the dominant process. The results from a simulation with $T_e = 5$ keV, and with the PF turned off, are shown in Fig. 9. In order to exceed greatly the required threshold intensity (cf. Fig. 1), ϵ was set to 50. This example, although it imposes somewhat unrealistic initial conditions, serves to illustrate some of the effects that distinguish ponderomotive self-focusing from thermal self-focusing. In Fig 9, aside from strong on-axis focusing, there is evidence of small-scale off-axis filamentary structures. The scale length of these structures depends, qualitatively, on the amplitude and width of filaments forming on the axis of the beam. For example, in Fig. 9(a) (time = 0.2 nsec) the most prominent filament has an intensity of 6×10^{18} Wcm^{-2}, and is relatively narrow. Several small-scale filaments are seen on a line moving radially outward from the main focus. In Fig. 9(b) (time = 0.6 nsec) the peak intensity of the filament is 5×10^{18} Wcm^{-2}, and its spatial extent has increased. Fewer small-scale structures are evident in this case. Finally, in Fig. 9(c) (time = 1.0 nsec) the peak intensity of the filament is 3.7×10^{18} Wcm^{-2}, and the scale length of the small-scale filaments has noticeably increased. The reason for the decrease in the filamented light intensity is that the plasma is rapidly heating. The temperature increases by 740 eV for the time interval shown. As the plasma heats, it becomes more difficult for narrow filaments to form (because of energy diffusion), and this results in less prominent off-axis intensity modulations.

Now we consider the more realistic case of a plasma with a temperature chosen low enough for thermal self-focusing to be more effective than ponderomotive self-focusing. When the temperature of the plasma is reduced, inverse bremsstrahlung absorption becomes more vigorous. The

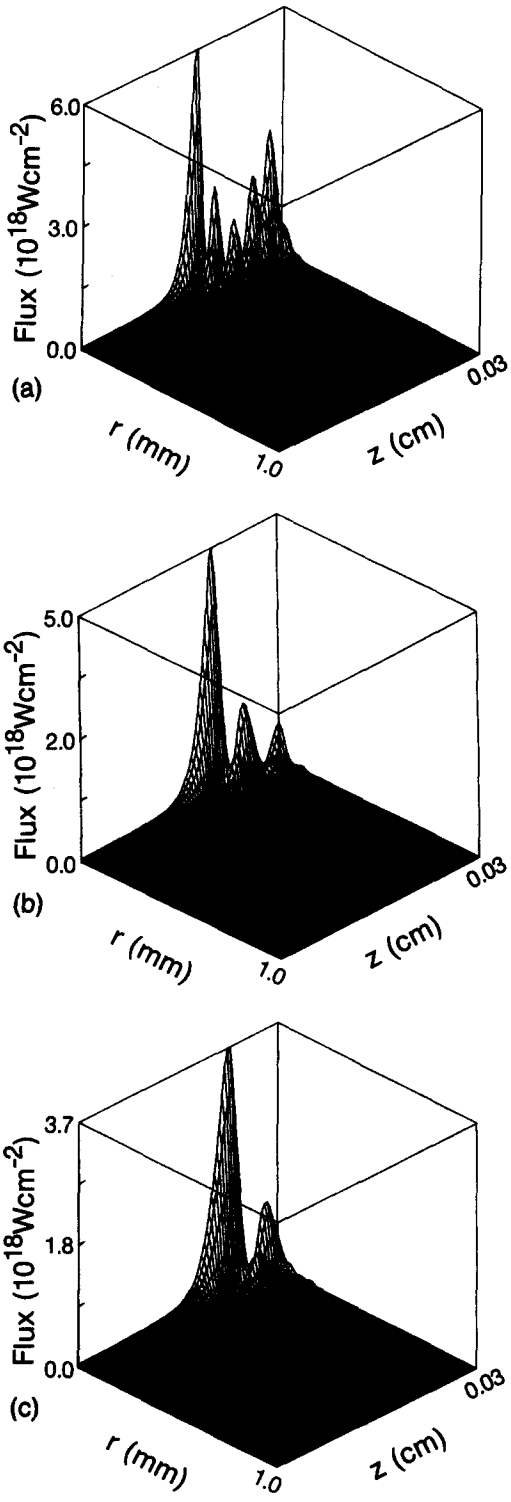

FIG. 9. Flux versus r and z with the PF turned off. Parameters used are (i) uniform intensity of 10^{15} Wcm^{-2}, (ii) $n_e/n_c = 0.1$, (iii) $\sigma = 100\,\mu$m, (iv) $\epsilon = 50$. The flux is shown at (a) $t = 0.2$ nsec, (b) $t = 0.6$ nsec, (c) $t = 1.0$ nsec.

plasma then absorbs heat locally at a much greater rate, and the threshold intensity for self-focusing drops. This occurs for a 1 keV initial plasma temperature. Under these conditions, with the PF off, a 100 μm radius Gaussian nonuniformity focuses at $\epsilon = 0.03$. At 5 keV, with the PF on, $\epsilon = 0.08$ is necessary for self-focusing to occur (cf. Fig. 5). The results of a simulation with a 1 keV plasma, and with the PF turned off, are shown in Fig. 10. The laser flux is shown at

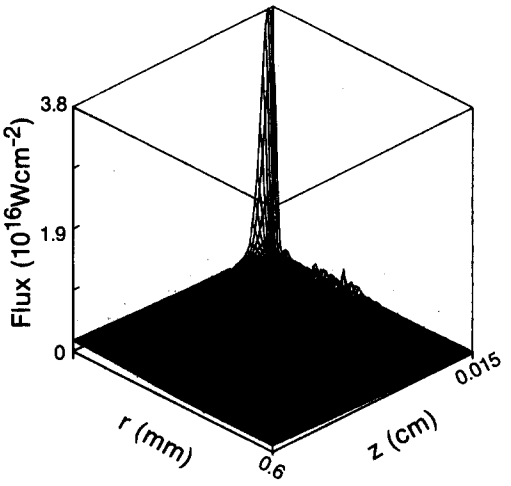

FIG. 10. Flux versus r and z with the PF turned off. Parameters used are the same as in Fig. 8, except that $T_e = 1$ keV. The flux is shown at $t = 1.0$ nsec.

a time of 1 nsec, when the position of the focus is about to exit the region of plasma simulated. As a result of inverse bremsstrahlung attenuation, at earlier times the beam self-focuses nearer to $z = 0$. However, after the plasma heats and expands, the light wave is able to penetrate farther along the z axis. In this example, we again observe off-axis intensity modulations resulting from pressure wave generation inside the high intensity focus. The progression of the laser focus along the z axis, with time, leaves behind a trailing "wake" of ion waves. The modulations closest to $z = 0$ therefore arose earliest in time, since they have propagated the farthest distance radially.

The above example is distinguished from the previous one by the initial temperature used. When the PF is neglected, and a high initial temperature is imposed (as in Fig. 9), it requires a large intensity to initiate self-focusing. For example, when $\sigma = 100$ μm (with $n_e/n_c = 0.1$), self-focusing first occurs when $\epsilon > 20$, i.e., at an intensity exceeding 2×10^{16} Wcm^{-2}. At 1 keV, the required value of ϵ is 0.03. In the former case, the spatial scale of the filamented light is greater, and the off-axis focusing is less noticeable. This occurs because the pressure difference between the heated region and the 5 keV surrounding plasma is much less than at 1 keV. More generally, we find that significant off-axis intensity variations (corresponding to $\delta n_e/n_e \leqslant 1\%$) occur when the intensity on the axis develops into one or more narrow intense spikes. There is evidence of this in Fig. 8(a) (which includes the PF), where the radial modulations of the flux are broad at the onset of self-focusing, relative to the structure observed after strong focusing has occurred [cf. Fig. 8(d)].

One conclusion to be drawn from the above results is that ion waves can be generated by thermal self-focusing or ponderomotive self-focusing. For the parameters considered here, however, it has been found that when the PF is included, the off-axis focusing is more prominent. At higher density and/or lower temperatures, the laser beam is more strongly attenuated, and the filamented light has a smaller intensity. The ponderomotive forces and localized heating associated with a filament, are less effective at driving ion waves. For example, simulations at $0.3n_c$, with T_e varying between 1 keV and 5 keV, showed significantly less amounts of off-axis focusing. Ion wave effects are therefore more pronounced in low density, relatively hot plasmas, as is the case in the outer corona of a laser-produced plasma.

V. SUMMARY AND CONCLUSIONS

A two-dimensional Eulerian hydrodynamic simulation code has been used to study self-focusing in a low density homogeneous hydrogen plasma. The incident laser beam was taken as the superposition of a uniform plane wave and a Gaussian nonuniformity. It is found that filamentation can drive ion waves near the axis of the laser beam. These ion waves can induce spatial and temporal modulations of the flux outside of the initial radius of the nonuniform beam. The small-scale filamentary structure on the laser beam is relatively unaffected by imposed changes in the amplitude and radius of the Gaussian nonuniformity, provided that the threshold intensity for self-focusing is exceeded. We have also investigated parameter ranges in which ponderomotive or thermal self-focusing dominates. Ion waves are generated irrespective of whether ponderomotive force effects are included or not. However, low density hot plasmas favor the generation of ion waves, and in such cases the ponderomotive force is responsible for the self-focusing.

The intensity threshold behavior of thermal and ponderomotively driven self-focusing has also been determined. Self-focusing was investigated in plasmas with densities varying from $0.1n_c$ to $0.3n_c$, and temperatures varying from 1 keV to 5 keV. At $0.1n_c$, neglecting ponderomotive forces, the threshold intensity is found to vary by approximately three orders of magnitude as the temperature is changed from 1 keV to 5 keV. When ponderomotive forces are included, they dominate self-focusing for $T_e \geqslant 1$ keV. The thermal self-focusing intensity threshold is limited by the electron thermal conduction mean free path. The associated energy diffusion out of the nonuniform beam becomes particularly important for spot sizes of less than 100 μm. Lowering T_e, or raising n_e, produces a similar effect: The incident beam is more strongly attenuated, and the threshold intensity subsequently rises. It is also found that hot spots with $\sigma \leqslant 50$ μm strongly self-focus in low density plasmas primarily because of the ponderomotive force.

ACKNOWLEDGMENTS

The authors would like to thank CRAY-CANADA for a generous donation of computer time. This work was supported by the Natural Sciences and Engineering Research Council of Canada.

[1] G. J. Pert, Plasma Phys. **20**, 175 (1978).
[2] D. W. Forslund, J. M. Kindel, K. Lee, E. L. Lindman, and R. L. Morse, Phys. Rev. A **11**, 679 (1975).
[3] K. G. Estabrook, E. J. Valeo, and W. L. Kruer, Phys. Fluids **18**, 1151 (1975).
[4] J. S. Pearlman and M. K. Matzen, Phys. Rev. Lett. **39**, 140 (1977).
[5] A. G. M. Maaswinkel, K. Eidmann, and R. Sigel, Phys. Rev. Lett. **42**, 1625 (1979).
[6] R. A. Cairns, Plasma Phys. **20**, 991 (1978).
[7] D. W. Forslund, J. M. Kindel, and E. L. Lindman, Phys. Rev. Lett. **30**, 739 (1973); Phys. Fluids **18**, 1002, 1017 (1975).

[8]C. S. Liu, M. N. Rosenbluth, and R. B. White, Phys. Fluids **17**, 1211 (1974).
[9]J. F. Drake, P. K. Kaw, Y. C. Lee, G. Schmidt, C. S. Liu, and M. N. Rosenbluth, Phys. Fluids **17**, 778 (1974).
[10]D. W. Phillion, E. M. Campbell, K. G. Estabrook, G. E. Phillips, and F. Ze, Phys. Rev. Lett. **49**, 2405 (1982).
[11]A. A. Offenberger, R. Fedosejevs, W. Tighe, and W. Rozmus, Phys. Rev. Lett. **49**, 371 (1982).
[12]K. Tanaka, L. M. Goldman, W. Seka, M. C. Richardson, J. Soures, and E. A. Williams, Phys. Rev. Lett. **48**, 1179 (1982).
[13]R. E. Turner, D. W. Phillion, B. F. Lasinski, and E. M. Campbell, Phys. Fluids **27**, 511 (1984).
[14]C. Joshi, T. Tajima, J. M. Dawson, H. A. Baldis, and N. A. Ebrahim, Phys. Rev. Lett. **47**, 1285 (1981).
[15]M. S. Sodha, A. K. Ghatak, and V. K. Tripathi, in *Progress in Optics*, edited by E. Wolf (North-Holland, Amsterdam, 1976), Vol. 13, p. 169.
[16]C. E. Max, Phys. Fluids **19**, 74 (1976).
[17]J. F. Lam, B. Lippman, and F. Tappert, Phys. Fluids **20**, 1176 (1977).
[18]D. Anderson and M. Bonnedal, Phys. Fluids **22**, 1839 (1979).
[19]R. Bingham and C. N. Lashmore-Davies, Plasma Phys. **21**, 433 (1979).
[20]A. B. Langdon and B. F. Lasinski, Phys. Rev. Lett. **34**, 934 (1975).
[21]S. Sartang, R. Evans, and W. T. Toner, J. Phys. D **16**, 955 (1983).
[22]R. S. Craxton and R. L. McCrory, J. Appl. Phys. **56**, 108 (1984).
[23]K. Estabrook, W. L. Kruer, and D. S. Bailey, Phys. Fluids **28**, 19 (1985).
[24]R. Marchand, R. Rankin, C. E. Capjack, and A. Birnboim, Phys. Fluids **30**, 1521 (1987).
[25]J. A. Stamper, R. H. Lehmberg, A. Schmidt, M. J. Herbst, F. C. Young, J. H. Gardner, and S. B. Obenschain, Phys. Fluids **28**, 2563 (1985).
[26]R. Rankin, R. Marchand, and C. E. Capjack, Bull. Am. Phys. Soc. **32**, 1797 (1987).
[27]S. V. Coggeshall, W. C. Mead, and R. D. Jones, Bull. Am. Phys. Soc. **32**, 1797 (1987).
[28]R. Rankin, A. Birnboim, R. Marchand, and C. E. Capjack, Comput. Phys. Commun. **41**, 21 (1986).
[29]J. N. McMullin, C. E. Capjack, and C. R. James, Phys. Fluids **21**, 1828 (1978).
[30]D. S. Kershaw, J. Comput. Phys. **26**, 43 (1978).
[31]J. P. Boris, in *Finite-Difference Techniques for Vectorized Fluid Dynamics Calculations*, edited by D. L. Book (Springer, New York, 1981), p. 29.
[32]J. A. Fleck, Jr., J. Comput. Phys. **16**, 324 (1974).